Journal of Solid State Chemistry 181 (2008) 1439–1444

Contents lists available at ScienceDirect

Journal of Solid State Chemistry

journal homepage: www.elsevier.com/locate/jssc

Rapid synthesis of tin (IV) oxide nanoparticles by microwave induced thermohydrolysis

J. Jouhannaud *, J. Rossignol, D. Stuerga

NANOSCIENCES-GERM (Groupe d'Etudes et de Recherches en Microondes), ICB (Institut Carnot de Bourgogne), UMR 5209 CNRS, Université de Bourgogne, 9 Avenue Alain Savary, B.P. 47870, 21078 Dijon Cedex, France

ARTICLE INFO

Article history:
Received 18 January 2008
Received in revised form
12 February 2008
Accepted 26 February 2008
Available online 26 March 2008

Keywords:
SnO_2
Microwave heating
Synthesis
Hydrothermal

ABSTRACT

Tin oxide nanopowders, with an average size of 5 nm, were prepared by microwave flash synthesis. Flash synthesis was performed in aqueous solutions of tin tetrachloride and hydrochloric acid using a microwave autoclave (RAMO system) specially designed by the authors. Energy dispersive X-ray analysis (EDX), X-ray powder diffraction (XRD), Brunauer–Emmett–Teller (BET) surface area analysis, nitrogen adsorption isotherm analysis, differential scanning calorimetry (DSC), thermogravimetric analysis (TGA), Fourier transform infrared (FTIR) spectroscopy, and transmission electron microscopy (TEM), were used to characterize these nanoparticles. Compared with conventional synthesis, nanopowders can be produced in a short period (e.g. 60 s). In addition, high purity and high specific surface area are obtained. These characteristics are fundamental for gas sensing applications.

1. Introduction

Tin(IV) oxide (SnO_2, rutile-type structure) is an n-type wide band gap (3.5 eV) semiconductor that presents a proper combination of chemical, electronic and optical properties that make it advantageous in several applications, such as catalysts [1,2], gas sensors [3,4], heat mirrors [5], varistors [6,7], transparent electrodes for solar cells [8], glass melting electrodes and optoelectronic devices [9]. Especially, SnO_2 nanoparticles have been intensively studied for gas sensing applications not only because of their relatively low operating temperature, but also due to the fact that they can be used to detect both reducing and oxidizing gases.

Nanoparticles of tin dioxide have been synthesized by various synthesis methods such as sol–gel [10], microemulsion [11], spray pyrolysis [12], gel combustion technique (i.e., Pechini method) [13], decomposition of an organometallic precursor [14], hydrothermal synthesis [15]. Among these methods, a conventionally accepted method is the synthesis from precursor hydroxides precipitated by the direct addition of bases (as NH_4OH) to tin chloride aqueous solutions ($SnCl_4$). Although this technique rapidly yields a large amount of powder but thermal annealing of powder is necessary to obtain high crystallinity. Consequently, surface area significantly decreases in relation to magnitude of thermal treatment (temperature and duration). Generally, powders with high surface area allow strong increase of gas sensors sensitivity.

Microwave-assisted synthesis is an emerging technology using the ability of microwave heating to accelerate chemical reactions. Some liquids and solids are able to transform electromagnetic energy into heating. Since the mid-90s more than 90 publications relating to inorganic synthesis have been published. Most of the reports of microwave-induced chemistry describe the use of commercial laboratory systems deriving from household microwaves. Numerous information about microwave–material interactions, dielectric properties, key ingredients for mastery of chemical microwave process and laboratory or pilot scale reactors should be found in [16] and [17] respectively.

Among various other inorganic compounds, SnO_2 powder has already been synthesized using microwave heating by Cirera et al. [18] and by Michel et al. [19]. These synthesis have been carried out by means of the RAMO system (French acronym of Reacteur Autoclave MicroOnde), which is an original microwave device designed by our research team [17]. Our microwave oven allows high electric field strength within heated samples compared to those of domestic oven or commercial device (CEM or Millestone). The heating system consists of a microwave generator, a waveguide and a resonant cavity loaded with the RAMO system. The microwave generator used is a continuous wave system (2.45 GHz) with microwave power up to 2 kW. The autoclave is made with polymer materials which are microwave transparent, chemically inert and sufficiently strong to accommodate the pressure induced. A fiber-optic thermometry system, a pressure transducer and a manometer allow to measure simultaneously

* Corresponding author. Fax: +33 380 39 61 32.
E-mail address: julien.jouhannaud@u-bourgogne.fr (J. Jouhannaud).

0022-4596/$ - see front matter © 2008 Elsevier Inc. All rights reserved.
doi:10.1016/j.jssc.2008.02.040

the temperature and the pressure within the reactor. Temperature measurements under microwave heating are very difficult and non-perturbing temperature sensor could be used. The system is controlled by pressure. The microwave power is adjusted in order to allow constant pressure within the vessel. A pressure release valve incorporated permits to use this experimental device routinely and safely. This experimental device is able to raise the temperature from ambient to 200 °C in less than 20 s (the pressure is close to 1.2 MPa and the heating rate is close to 5 °C s^{-1}). This device is able to produce rapid bulk heating. Due to strong thermal gradients induced by microwave heating, strong stirring occurs for liquids leading to thermal uniformity of heated medium. Hence, it combines advantages of forced hydrolysis (homogeneous precipitation) and very fast heating rate. Our device system has allowed production of various nanomaterials such as iron oxides [20], zirconia [21,22], titanium oxide [23], tin oxide [19], nanocomposites [24,25], manganese oxide [26] and more recently nickel ferrite [27]. The RAMO system associates advantages of solution nucleation processes with core heating and heating rate induced by microwave heating.

Contrary to our previous work restricted to colloidal tin oxide [28], the aim of the present work was to prepare SnO_2 nanocrystalline powder with high surface area by microwave-induced thermohydrolysis. Conventional operating conditions are generally based on salts aqueous solutions using hydroxide precipitation induced by pH increase. The aim of this work is the study of microwave induced thermohydrolysis within acidic solutions (hydrochloric acid). Obviously, the products will be compared with those prepared with the others microwave conditions [24,26,29,30]. The various nanopowders produced were characterized by energy dispersive X-ray analysis spectrometer (EDXS), X-ray diffraction (XRD), Brunauer–Emmett–Teller (BET) surface area analysis, thermogravimetric analysis (TGA), differential scanning calorimetry (DSC), Fourier transform infrared (FTIR) spectroscopy and transmission electron microscopy (TEM).

1.1. Operating conditions

Our simplest method for the generation of tin (IV) oxide nanoparticules is based on microwave thermohydrolysis of metal salt solutions [17,21–24]. It is well known that most polyvalent cations as tin (IV) readily hydrolyze, and that deprotonation of coordinated water molecules is greatly accelerated with increasing temperature. Since hydrolysis products are intermediates to precipitation of metal oxides, these species can be generated at the proper rate to eventually yield nanoparticles by the adjustment of heating rate, temperature and pH. The mechanism of hydroxylation or olation reaction involves a scheme given by

$$[Sn(OH_2)_6]^{4+} + hH_2O \rightarrow [Sn(OH)_h(OH_2)_{6-h}]^{(4-h)+} + hH_3O^+ \quad (1)$$

whereas the oxolation reaction involves a scheme given by

$$n[Sn(OH)_h(OH_2)_{6-h}]^{(4-h)+} + qH_2O \rightarrow [Sn_n(OH)_{nh+q}(OH_2)_{n(6-h)-q}]^{(n4-nh-q)+} + qH_3O^+ \quad (2)$$

Obviously, these complexes act as precursors to nucleation and they affect the particle growth. The composition and the rate of generation of these species, controlled by heating rate, will determine the chemical and physical natures of the resulting precipitate. The authors have defined operating conditions able to facilitate concomitant olation and oxolation reactions for tin (IV) precursor. Hence, the general balance of the reactional scheme is given by

$$SnCl_4 + 6H_2O \rightarrow SnO_2 + 4H_2O + 4HCl \quad (3)$$

According to this reaction scheme, side product is hydrochloric acid leading to more acidic solutions after microwave treatment.

2. Experimental

2.1. Preparation

The reaction media were constituted by tin tetrachloride aqueous solutions with hydrochloric acid. Tin (IV) chloride (99.995%, Aldrich) and hydrochloric acid (Prolabo, RP Normapur) were used without further purification. Addition of tin (IV) chloride has been done under vigorous stirring, in previously acidified water. The hydrochloric acid concentration is fixed at 0.1 mol L^{-1} and the tin salt concentrations are 0.1 and 0.08 mol L^{-1}. Table 1 summarizes samples data (name, concentration of tin chloride, holding time, microwave power and annealing temperature). The sample A was annealed under different temperatures in order to obtain samples B, C, D and E. Samples F, G and H only differ in microwave holding time whereas samples I and J have different tin chloride concentrations. For each experiment, 25 mL of the solution is placed in a Teflon® flask inserted within a polyetherimide flask. This reactor was quickly sealed and an argon pressure introduced (0.5 MPa). The solution was submitted to microwave irradiation with the RAMO system describes in Fig. 1.

Table 1
Nomenclature and operating conditions for synthesis of tin (IV) oxide

Sample name	$[SnCl_4]$ (mol L^{-1})	[HCl] (mol L^{-1})	Time (s)	Initial power (kW)	Temperature of heat treatment (°C)
A	0.1	0.1	60	1	None
B	0.1	0.1	60	1	200
C	0.1	0.1	60	1	400
D	0.1	0.1	60	1	600
E	0.1	0.1	60	1	800
F	0.1	0.1	45	1	None
G	0.1	0.1	60	0.75	None
H	0.1	0.1	120	1	None
I	0.08	0.1	45	1	None
J	0.08	0.1	60	1	None

Fig. 1. Presentation of microwave autoclave reactor RAMO.

The microwave treatment was decomposed in two steps. During the first step, the microwave power (1 KW) is applied until the pressure reaches a threshold value of 0.9 MPa. This pressure corresponds to a temperature close to 180 °C. The heating rate is close to 5 °C s^{-1}. During the second step, this pressure threshold was kept by monitoring the microwave power. Holding times are between 60 and 120 s. Fig. 2 illustrates the relationship between temperature and pressure rates generated within the reactor for the reactants used.

After microwave treatments, powders were centrifuged and washed with distilled water in order to eliminate hydrochloric acid and chloride ions. They were dried at room temperature.

2.2. Characterization

Characterization was performed to determine structure and composition of the end-powders. Possible contaminations by chloride ions Cl^- are specially studied. Chemical compositions were conducted on a JEOL JEM-2100 LaB_6 transmission electron microscope fitted with an EDXS JEOL JED 2300 T.

The structure of the samples was verified by XRD. XRD measurements were done with an INEL diffractometer equipped with a CPS 120 curved position sensitive X-ray detector. The CuK_α radiation from a Cu anticathode tube was selected by a graphite monochromator and used as the X-ray source. Diffraction measurements were done with a fixed grazing incidence angle, $\omega = 1°$, in order to enhance the signal coming from the films with respect to that corresponding to the substrate.

Specific surface area of powders was measured by BET isotherm technique with nitrogen adsorption (Autosorb-1 Quantachrome). Samples (150–200 mg of powder) are outgassed at 100 °C. The BET method is used in calculation of surface area values from the isotherm of nitrogen adsorption [31].

Thermal properties of samples were examined by TGA and DSC (TGA–DSC; model SDT 2960, TA Instruments, Inc.) with heating rate equal to 10 °C min^{-1} up to 400 °C, in N_2 flowing gas at first. Data acquisition was performed on-line.

FTIR spectra of the samples were recorded with a Bruker Vector 22 equipped with a Specac Golden Gate^{TM} ATR device and working in a spectral range of 4000–400 cm^{-1}, with a resolution of 2 cm^{-1}. The pellets were a mixture of 200 mg of KBr dried at 120 °C, and 3 mg of studied sample.

Finally, the morphology and the microstructure of the powders were studied with a JEOL JEM-2100 LaB_6 TEM with a 200 keV accelerating voltage. The samples were prepared by dispersing some powder within ethanol, a drop of the dispersion placed on a copper grid coated with a layer of amorphous carbon.

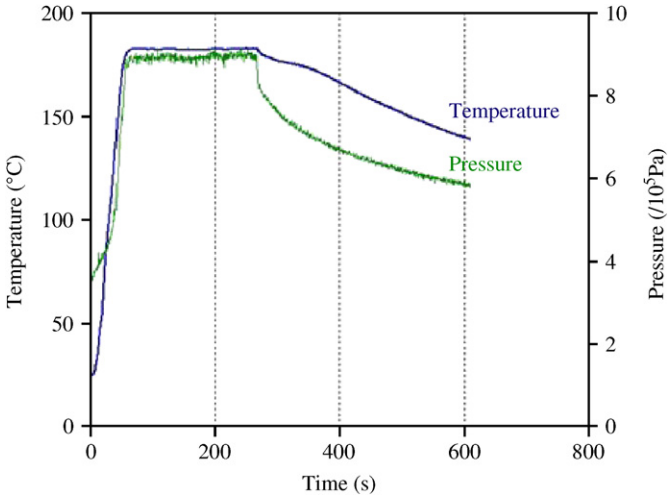

Fig. 2. Evolution of temperature and pressure vs. time. Initial power: 1 kW.

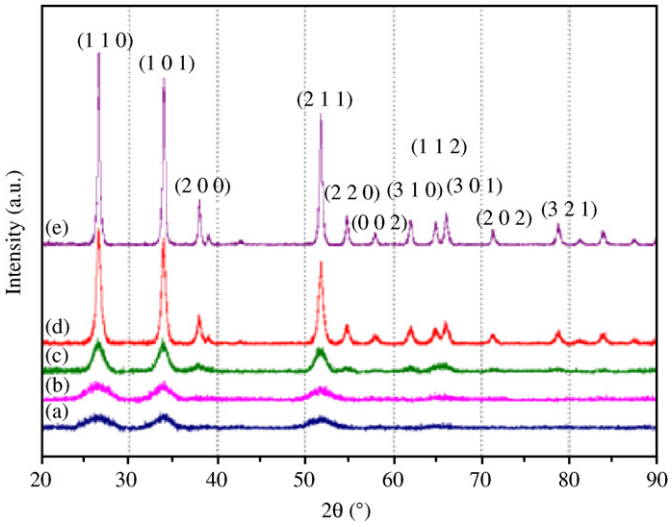

Fig. 3. XRD patterns of SnO_2: (a) as-prepared SnO_2 (sample A), (b) annealing at 200 °C (sample B), (c) 400 °C (sample C), (d) 600 °C (sample D) and (e) 800 °C (sample E).

3. Results and discussion

3.1. Structural analysis

The structure and purity of the nanoparticles were firstly determined by the XRD. Tin oxide has cassiterite structure with tetragonal framework lattice (rutile type structure) with $a = 4.7382(4)$ Å, $c = 3.1871(1)$ Å and the space group $P42/mnm$. Sn^{4+} and O^{2-} ions are in 2*a* and 4*f* positions, respectively. Fig. 3 shows the XRD patterns of samples before (raw powder) and after annealing treatment under different temperatures. The XRD pattern of raw powders (sample A) showed the presence of very broad peaks (Fig. 3, curve (a)), indicating particles with small crystalline size. All diffraction lines are assigned well to cassiterite tetragonal crystalline phase of SnO_2 with a reference pattern of JCPDS (41-1445). The average crystal sizes are close to 5 nm for sample A, according to the Debye-Scherrer formula based on the (110) reflection. Annealing treatment were applied to sample A at 200 °C (sample B), 400 °C (sample C), 600 °C (sample D), and 800 °C (sample E). Holding time is equal to 2 h. Due to the annealing treatment, the diffraction peaks become narrower and stronger due to the fact that the average crystal sizes increase. Crystallinity is significantly improved. The average crystal sizes are 6, 9, 21 and 33 nm for samples B, C, D and E, respectively. Samples F to J exhibit same XRD patterns than the sample A.

The cassiterite structure of the SnO_2 samples is confirmed by the FTIR spectra (Fig. 4-1). Two bands at ca. 660 and 540 cm^{-1} for raw sample are observed. Magnitude of the peak at 540 cm^{-1} decreases gradually with the annealing temperature increasing. After calcination at 600 °C (sample D), the peak almost disappears and a new peak appears at ca. 610 cm^{-1}. This band is assigned to the antisymmetric Sn–O–Sn stretching mode of the surface-bridging oxide formed by condensation of adjacent surface hydroxyl groups (which produce water). After annealing at 600 °C (sample D), a small peak appears at 470 cm^{-1}, which is assigned to the symmetric Sn–O–Sn stretching mode [32,33].

The energy dispersion X-ray (EDX) spectrum is used to confirm the composition of samples. Typical EDX pattern for sample A is presented in Fig. 4-2, indicates high purity. The presence of C and

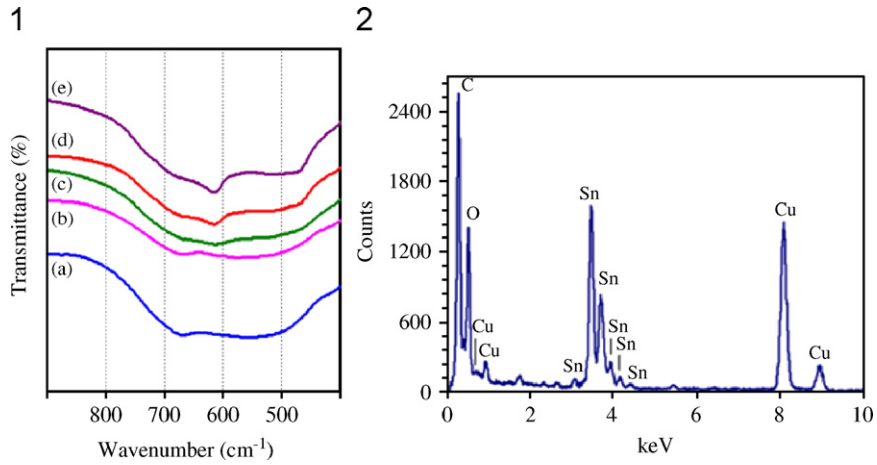

Fig. 4. (1)–FTIR spectra of SnO_2: (a) as-prepared SnO_2 (sample A), (b) annealing at 200 °C (sample B), (c) 400 °C (sample C), (d) 600 °C (sample D) and (e) 800 °C (sample E). (2)—EDX pattern of SnO_2 (sample A).

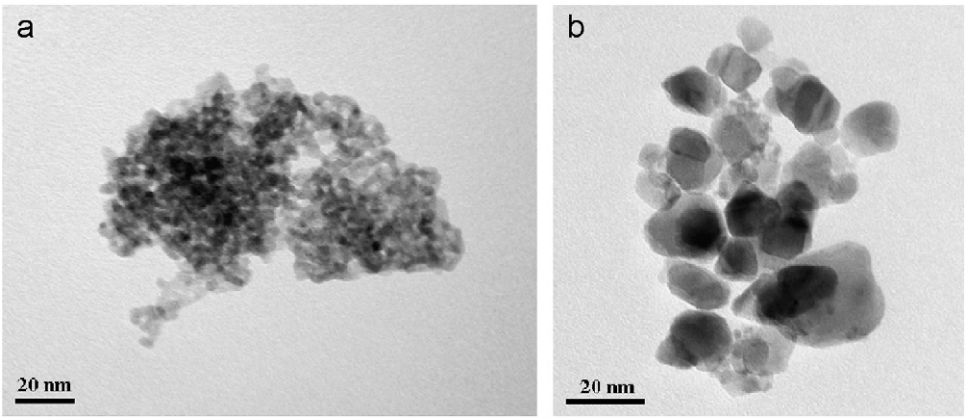

Fig. 5. TEM images of SnO_2: (a) as-prepared SnO_2 (sample A), (b) calcined at 600 °C (sample D).

Cu is due to the copper grid coated with a layer of amorphous carbon. Other samples show almost the same pattern. Similar elemental compositions are observed with all samples. EDX analysis shows that no Cl^- ions are present in the powders. Moreover, Ocaña et al. [34,35] have demonstrated that the presence of Cl^- ions is revealed by a shoulder at 435 cm^{-1} which refers mainly to the Sn–Cl vibrations. No peak is observed at 435 cm^{-1} on the FTIR spectra (Fig. 4-1).

3.2. Morphological and surface analysis

Fig. 5 presents the TEM observations for sample A (raw powder) and sample D (annealing temperature 600 °C). A typical TEM image of raw powder is given in Fig. 5a. The sample is constituted by nanoparticles very similar with average size close to 5 nm. The powder annealed at 600 °C (Fig. 5b) shows similar results with an average particle size of 21 nm. The results obtained are in good agreement with the sizes estimated by XRD. The same morphological shape is observed for the others samples.

The surface area of raw powder was estimated by BET technique. Prior to the measurement, the samples were degassed at 100 °C under vacuum for at least 2 h. The nitrogen adsorption at −196 °C leads to relatively high specific surface area from 166 to 191 $m^2 g^{-1}$ (Table 2). Diameters are estimated close to 5 nm with assuming spheroids particles for all the studied samples. Results show that the morphology of the nanoparticles (spherical shaped) are not influenced by the operating conditions (microwave holding time and power, tin chloride concentrations). The results obtained are in good agreement with the particle sizes estimated by XRD and TEM.

Table 2
Specific surface area and average particle size from BET

Sample name	Specific surface area ($m^2 g^{-1}$)	Average particle size from BET (nm)
A	185 ± 5	4.6 ± 0.3
F	175 ± 5	4.9 ± 0.3
G	166 ± 5	5.2 ± 0.3
H	191 ± 5	4.5 ± 0.3
J	171 ± 5	5.0 ± 0.3

Fig. 6-1 shows the results of thermogravimetric analysis of sample A and heat-treated powders (samples B, C, D and E) performed over the temperature of 25–550 °C in an N_2 atmosphere. Concerning the sample A, the particles show a total weight loss (9.0%) between 50 and 550 °C. A first weight loss (3.0%) is detected from 50 to 150 °C. It may come from the evaporation of physically adsorbed water in the particles. The greatest rate of weight loss (6.0%) was observed between 150 and 550 °C, which can be attributed to the continuous removal of chemically adsorbed water, which may be related to different types of surface hydroxyl group condensation [36]. Above 650 °C, no

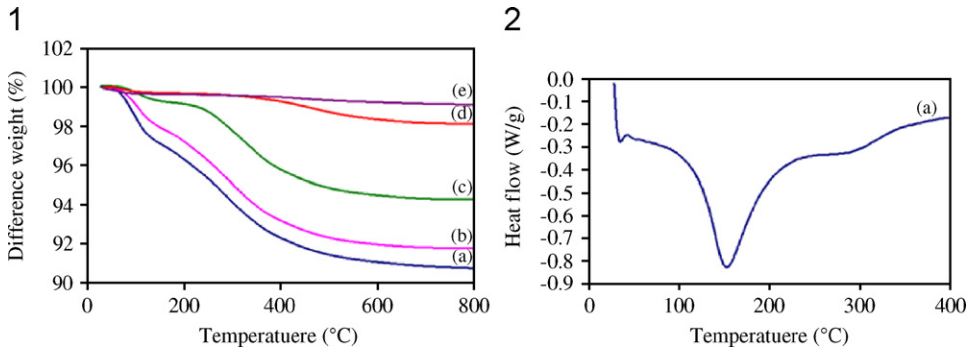

Fig. 6. TGA curves (1) and DSC curves (2) of SnO_2: (a) as-prepared SnO_2 (sample A), (b) annealing at 200 °C (sample B), (c) 400 °C (sample C), (d) 600 °C (sample D) and (e) 800 °C (sample E).

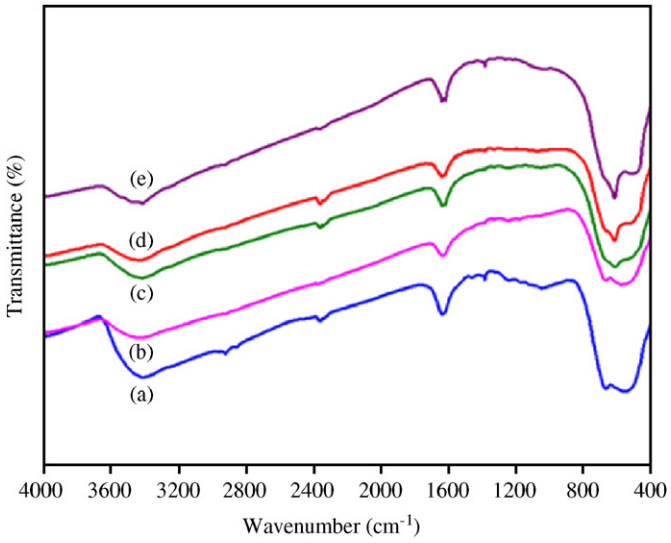

Fig. 7. FTIR spectra of SnO_2: (a) as-prepared SnO_2 (sample A), (b) annealing at 200 °C (sample B), (c) 400 °C (sample C), (d) 600 °C (sample D) and (e) 800 °C (sample E).

weight loss is observed in the TGA curve. Similar curves are obtained with the other samples. A decrease of the magnitude weight loss is observed with the increase of the annealing temperature. The presented DSC curve (Fig. 6-2) shows an endothermic peak at a temperature of 150 °C. It gives evidence of evaporation of physically adsorbed water within the particles.

Fig. 7 shows the FTIR spectra of raw powder (sample A). The weak peaks in the range 850–1350 cm^{-1} and 2300–2900 cm^{-1} are probably due to the fact that the spectra were not recorded in situ and some adsorption of water or CO_2 from the ambient atmosphere has occurred. The bands observed in the range 850–1350 cm^{-1} may be assigned to a hydroxyl-bending mode of different types of surface hydroxyl groups [37] and the weak peaks at 2852 cm^{-1} and 2923 cm^{-1} belong to the stretching vibrations of -H bonds. These results show that there is a little amount of water adsorbed on each sample. The results obtained are confirmed by the TGA curves.

4. Conclusion

SnO_2 nanopowders were synthesized by microwave flash synthesis performed in tin tetrachloride aqueous acidic solutions. Raw powders obtained have specific surface area from 166 to 191 $m^2 g^{-1}$ with average particle sizes close to 5 nm, whatever the holding time of synthesis used in this work. Crystallites sizes increased in relation to annealing temperature 6, 9, 21 and 33 nm for 200, 400, 600 and 800 °C, respectively. Moreover, average size is slightly small. These sizes, estimated by XRD, are confirmed by the TEM and BET. Despite use and production of hydrochloric acid according to reaction scheme (Eq. (3)), no trace of chloride ions has been detected within raw powder. Compared to our previous work relating to colloidal form of tin oxide suspension [28], these new operating conditions allow production of powder able to be used for gas sensor. Reaction rate is close to 70% (sample F-45 s), 85% (sample G-60 s; sample H-120 s). Consequently, reaction time is close to 60 s. Obviously, an increase of precursor concentration induce a rate enhancement: 65% for sample J (0.08 mol L^{-1}) and 85% for sample A (0.1 mol L^{-1}). The reaction process leads to spherical shaped particles with diameter close to 5 nm. These particles are obtained whatever the microwave holding time or tin chloride concentration. Typical experiments lead in few minutes to 500 mg of tin oxide powder with higher surface area. Compared to conventional processes, our new protocol does not imply annealing treatment in order to transform amorphous hydroxides and oxy-hydroxides into oxide. Moreover, our process directly leads to aqueous suspensions of tin oxide nanoparticles. These suspensions could be used for coating or casting. However, the agglomerate capability should be evaluated soon.

Due to high value of specific surface area, our powders could offer high sensitivity to gas sensor compared to conventional powder. This point will be studied in the immediate future. Further work will be presented to give a better understanding on the microstructure of our powders. More investigations concerning the morphology study of these powders by Transmission Electron Microscopy will be published soon.

Acknowledgments

The authors wish to acknowledge the Regional Council of Burgundy for his financial support. They are also grateful to Farouk Azzaz, Remy Chassagnon and Marie-Laure Leonard for their help in BET, MET/EDX and TGA/DSC experiments respectively, from the Institut Carnot Bourgogne.

References

[1] S. Wang, J. Huang, Y. Zhao, S. Wang, S. Wu, S. Zhang, W. Huang, Mater. Lett. 60 (2006) 1706.
[2] J. Wöllenstein, H. Böttner, M. Jaegle, W.J. Becker, E. Wagner, Sensors Actuators B 70 (2000) 196.
[3] J. Kaur, S.C. Roy, M.C. Bhatnagar, Sensors Actuators B 123 (2007) 1090.
[4] H.C. Wang, Y. Li, M.J. Yang, Sensors Actuators B 119 (2006) 380.
[5] M. Kojima, F. Takahashi, K. Kinoshita, T. Nishibe, M. Ichidate, Thin Solid Films 392 (2001) 349.
[6] A. Mosquera, J.E. Rodríguez-Páez, J.A. Varela, P.R. Bueno, J. Eur. Ceram. Soc. 27 (2007) 3893.

[7] M.R. Cássia-Santos, V.C. Sousa, M.M. Oliveira, F.R. Sensato, W.K. Bacelar, J.W. Gomes, E. Longo, E.R. Leite, J.A. Varela, Mater. Chem. Phys. 90 (2005) 1.
[8] T. El Moustafid, H. Cachet, B. Tribollet, D. Festy, Electrochem. Acta 47 (2002) 1209.
[9] T.W. Kim, D.U. Leea, D.C. Chooa, J.H. Kima, H.J. Kima, J.H. Jeonga, M. Junga, J.H. Bahangb, H.L. Parkb, Y.S. Yoonc, J.Y. Kimd, J. Phys. Chem. Solids 63 (2002) 881.
[10] M.A. Dal Santos, A.C. Antunes, C. Ribeiro, C.P.F. Borges, S.R.M. Antunes, A.J. Zara, S.A. Pianaro, Mater. Lett. 57 (2003) 4378.
[11] K.C. Song, J.H. Kim, J. Colloid Interf. Sci. 212 (1999) 193.
[12] J.H. Lee, S.J. Park, J. Am. Ceram. Soc. 76 (1993) 777.
[13] M. Bhagwat, P. Shah, V. Ramaswamy, Mater. Lett. 57 (2003) 1604.
[14] C. Nayral, E. Viala, V. Collière, P. Fau, F. Senocq, A. Maisonnat, B. Chaudret, Appl. Surf. Sci. 164 (2000) 219.
[15] C. Guo, M. Cao, C. Hu, Inorg. Chem. Commun. 7 (2004) 929.
[16] D. Stuerga, A. Loupy (Eds.), Microwave in Organic Synthesis, Wiley, ISBN 3527314520, 2006 (Chapter 1).
[17] B. Ondruschka, W. Bonrath, D. Stuerga, Microwave in Organic Synthesis, Wiley, ISBN 3527314520, 2006 (Chapter 2).
[18] A. Cirera, A. Vila Vilà, A. Diéguez, A. Cabot, A. Cornet, J.R. Morante, Sensors Actuators B 64 (2000) 65.
[19] E. Michel, D. Stuerga, D. Chaumont, J. Mater. Sci. Lett. 20 (2001) 1593.
[20] K. Bellon, P. Rigneau, D. Stuerga, Eur. Phys. J. Appl. Phys. 7 (1999) 41.
[21] K. Bellon, D. Stuerga, D. Chaumont, J. Mater. Res. 16 (2001) 2619.
[22] L. Combemale, G. Caboche, D. Stuerga, D. Chaumont, Mater. Res. Bull. 40 (2005) 529.
[23] E. Michel, D. Stuerga, D. Chaumont, J. Colloid Interf. Sci. 285 (2005) 674.
[24] T. Caillot, D. Aymes, D. Stuerga, N. Viart, G. Pourrov, J. Mater. Sci. 37 (2002) 5153.
[25] T. Caillot, G. Pourroy, D. Stuerga, J. Solid State Chem. 177 (2004) 3843.
[26] C. Bousquet-Berthelin, D. Stuerga, J. Mater. Sci. Lett. 40 (2005) 253.
[27] C. Bousquet-Berthelin, D. Stuerga, J. Solid State Chem. 181 (2008) 616.
[28] E. Michel, D. Stuerga, D. Chaumont, J. Colloid Interf. Sci. 257 (2003) 258.
[29] J.H. Lee, C.K. Kim, S. Katoh, R. Murakami, J. Alloys Compd. 325 (2001) 276.
[30] C.K. Kim, J.H. Lee, S. Katoh, R. Murakami, M. Yoshimura, Mater. Res. Bull. 36 (2001) 2241.
[31] S. Brunauer, P. Emmett, E. Teller, J. Am. Chem. Soc. 60 (1938) 309.
[32] P.G. Harrison, A.J. Guest, J. Chem. Soc., Faraday Trans. 83 (1987) 3383.
[33] P.G. Harrison, N.C. Lloyd, W. Daniell, C. Bailey, W. Azelee, Chem. Mater. 11 (1999) 896.
[34] M. Ocana, C.J. Serna, J.V. Garcia-Ramos, E. Matijevic, Solid States Ionics 63 (1993) 170.
[35] M. Ocana, C.J. Serna, E. Matijevic, Mater. Lett. 12 (1991) 32.
[36] M. Majdoub, A. Loupy, A. Petit, S. Roudesli, Tetrahedron 52 (1996) 617.
[37] C.P. Sibu, S.R. Kumar, P. Mukundan, K.G.K. Warrier, Chem. Mater. 14 (2002) 2876.